PERGAMON

International Journal of Solids and Structures 38 (2001) 915–934

INTERNATIONAL JOURNAL OF SOLIDS and STRUCTURES

www.elsevier.com/locate/ijsolstr

Nonlinear stability of simplified structural models simulating elastic shell panels of revolution under step loading

D.S. Sophianopoulos *

Department of Civil Engineering, National Technical University of Athens, 42 Patision Street, 106 82 Athens, Greece

Received 8 October 1999; in revised form 23 February 2000

Abstract

The present investigation deals with the nonlinear analysis of the dynamic buckling response and global stability aspects of two 3-DOF spring-mass, initially imperfect dissipative simplified structural models under step loading, simulating elastic shell panels of revolution and in particular a spherical cap and a conical panel. It is found that snapping, which is the main characteristic of the actual continuous structures, is successfully captured by the proposed simulations, which following a straightforward nonlinear approach are found to exhibit dynamic snap-through buckling, associated with a point attractor response in the large, implying global stability. Furthermore, the presence of physically not accepted complementary equilibrium configurations does not affect the long term response of the autonomous systems dealt with, but only complicates the motion and elongates the time before the final steady state. Finally, the criterion of zero total potential energy yields excellent lower bounds of the exact dynamic buckling loads, very important for structural design purposes.

Keywords: Structural models; Dynamic snap-through; Point attractors; Global stability; Shells of revolution

1. Introduction

The strongly nonlinear and imperfection-sensitive behavior of shell structures under various types of dynamic loading or excitation, leading to catastrophic failure in some circumstances, has been the subject of numerous investigations, especially over the last 40 years. More specifically, studies dealing with the dynamic response of such structures have revealed a variety of interesting phenomena, depending on the shape and geometry of the shell considered, its properties and control parameters involved, as well as the type of the loading. Among these, one should refer to interaction of competing buckling modes and alternation of the membrane stress distribution as imperfections grow (Galladine, 1995), cusp-catastrophe and snap-through buckling (Ye et al., 1995), dynamic snap-out instability (Akkas, 1978) and chaotic snapping behavior (Greer and Palazotto, 1995), "strange" phenomena, periodic and/or random-like

* Fax: +30-1-772-3442.

E-mail address: dimisof@central.ntua.gr (D.S. Sophianopoulos).

0020-7683/01/$ - see front matter
PII: S0020-7683(00)00062-7

chaotic oscillations (Karaesmen et al., 1992), dynamic instability in a secondary displacement state-parametric resonance (Chien and Palazotto, 1992), etc.

Although the governing differential equations of motion are nonlinear and coupled in nature, the rapid development of analytical techniques and numerical methods combined with the advent of powerful computers, have enabled scientists to cast new light upon the global response and the corresponding buckling characteristics of shells. In as much as, for the dynamic buckling analysis of the aforementioned type of structures, it has been shown and evidently reported (Akkas, 1976; Simitses, 1990) that the most severe case of dynamic loading is the step load of infinite duration, while for shell panels of revolution (axishells, Libai and Simmonds, 1998) subjected to a concentrated step load, it is widely believed that the generalized displacement associated with the degree of freedom of the concentrated load dominates the system's behavior. Furthermore, in conjunction with the last two pertinent remarks, engineering practice often overcomes the mathematical and other difficulties arising, when dealing directly with the nonlinear dynamics of actual continuous structures, simulating the latter via simple models with a few degrees of freedom. This is achieved with the comprehensive use of various matching criteria, provided that these embrace the salient and prominent features of the structures modeled (Kounadis, 1994). Namely, such simple models by no means posses the fidelity of corresponding sophisticated Finite Element Method (FEM) ones but both experimental and theoretical findings point out that the majority of the nonlinear characteristics of continuous structures may be simulated quite adequately.

In addition to the above, shells of revolution, thought of mainly as conical plane cut-off sections – except perhaps deep conical caps, contain a rather convenient and easy to describe geometry, and consequently their nonlinear dynamic buckling response may be successfully simulated qualitatively through the use of simple models. The comprehensive modeling of the nonlinear response of these structures, acted upon by a transverse, constant directional, conservative step point loading of infinite duration, with significant membrane activity and elastic nature, i.e. elastic shell panels, is the subject of the present study. Based on

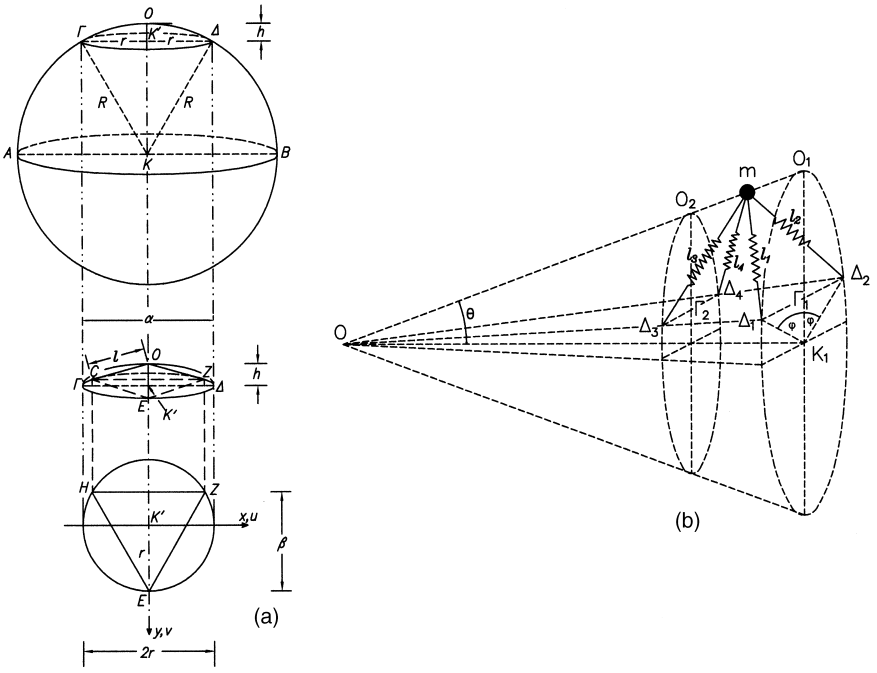

Fig. 1. Geometry and sign convention of a (a) spherical cap and (b) conical shell panel.

previous similar studies, dealing with cylindrical shell panels (Chien and Palazotto, 1992; Greer and Palazotto, 1995; Kounadis and Sophianopoulos, 1996), this investigation focuses on the analysis of two 3-DOF spring-mass dissipative simplified structural models, both initially imperfect, reported recently as simulations of the nonlinear behavior of spherical and conical shell panels (Michaltsos et al., 1996, 1998).

After establishing and manipulating the strongly nonlinear Lagrange equations of motion, employing a straightforward dynamic buckling approach, it is found that the shell panels dealt with, which under statically applied load exhibit as outlined in the citations given earlier, a limit point instability, buckle dynamically through a saddle or its vicinity of the postbuckling physical unstable equilibrium path. After limited in time and amplitude oscillations about this fixed point, the motion of the systems escapes and is finally attracted by remote stable, also physical, equilibria exhibiting a point attractor response largely, which implies global dynamic stability. The pertinent zero total potential energy criterion and the dynamic buckling analysis developed by Kounadis (1993, 1994, 1996), fully and readily applicable for the models under consideration, yield excellent lower bound buckling estimates, of great importance for engineering design purposes; thus, a further investigation of the motion channel geometry with more refined approximations as in Kounadis and Sophianopoulos (1996) are no longer necessary. Finally, although there seems to a certain level an intermediate effect of complementary physically not accepted equilibrium configurations, these do not affect the long term response, but only complicate and delay the motion before it settles on its remote attractor. Thus, contrary to previous findings (Chien and Palazotto, 1992) and although the proposed models could capture possible coupling effects, parametric resonance does not occur, neither quasi-periodic nor chaotic motions are encountered, since all these are ruled out due to the whole autonomous formulation, based on a well-behaved potential function.

2. Description of the models

According to the geometry and sign-displacement convention of a spherical cap and a conical shell panel depicted in Fig. 1(a, and b, respectively), the corresponding three and four spring, one-mass, 3-DOF models shown in Fig. 2(a) and (b) are adopted, acted upon by a vertical step loading of infinite duration on the center of mass m. Both the models illustrated in Fig. 2 represent the perfect configurations for reasons only of clarity. The multiple symmetries of the sphere allow the Spherical Cap Model to consist of three identical linearly elastic springs, while on the other hand the existence of only one symmetry plane in the cone leads

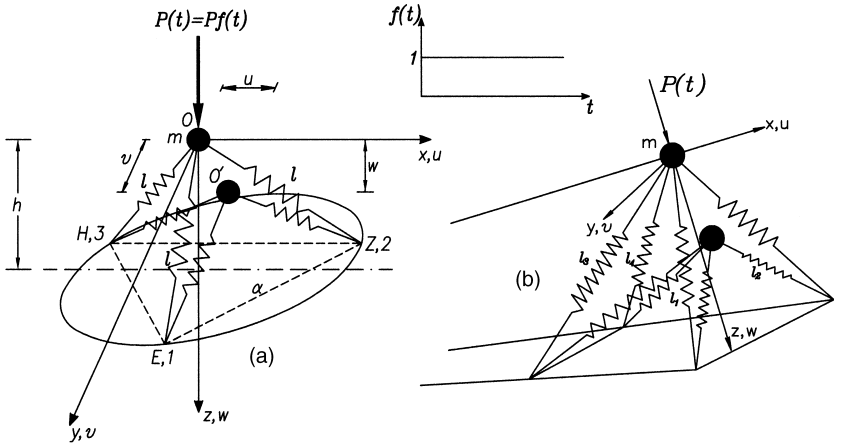

Fig. 2. Proposed 3-DOF models of a (a) spherical cap and (b) conical shell panel, under step loading of infinite duration.

to the use of two pairs of similarly identical springs, for the corresponding Conical Shell Panel Model. For the sake of simplicity the abbreviations SCM and CSPM will be used in the subsequent analysis. Since the correct and realistic simulation of everyday practice real structures must include initial imperfections and damping, both SCM and CSPM contain springs with stiffnesses k_i ($i=1$–3 or 4) with corresponding dashpots having Rayleigh type damping coefficients c_i ($i=1$–3 or 4) and are characterized by an initial unstressed trivial configuration, given by imperfection displacement components u_0, υ_0 and w_0. Therefore, the degrees of freedom utilized are strictly translational, i.e. no rotation and thus no bending action is present. In this manner, the models dealt with may as well capture the most significant feature inherent in the buckling response of relatively deep shell structures, for which membrane activity is pronounced, for the nonlinear dynamic analysis to follow. For a more detailed description of the proposed models one may refer to the relevant citations (Michaltsos et al., 1996, 1998).

3. Geometric considerations

Let us consider the perfect models of Fig. 2; if under the action of the point load, the new position of the origin is now defined by displacement components u, υ, w, one can write the new lengths of the stressed springs, for each model, as follows:

3.1. Spherical cap model

$$\ell_{D1}=\left\{u^2+(r-\upsilon)^2+(h-w)^2\right\}^{1/2},$$

$$\ell_{D2}=\left\{\left[\frac{r\sqrt{3}}{2}-u\right]^2+\left[\frac{r}{2}+\upsilon\right]^2+(h-w)^2\right\}^{1/2},\qquad h^2+r^2=\ell^2, \tag{1a–c}$$

$$\ell_{D3}=\left\{\left[\frac{r\sqrt{3}}{2}+u\right]^2+\left[\frac{r}{2}+\upsilon\right]^2+(h-w)^2\right\}^{1/2}.$$

3.2. Conical shell panel model

$$\ell_{Di}=\left\{(x\ell_i-u)^2+(y\ell_i-\upsilon)^2+(z\ell_i-w)^2\right\}^{1/2},\quad i=1\text{–}4, \tag{2a–d}$$

where

$$\begin{aligned}
&x\ell_1=x\ell_2=\frac{h}{2\cos\theta}-H\tan\theta(1-\cos\phi)\sin\theta,\\
&x\ell_3=x\ell_4=-\frac{h}{2\cos\theta}-(H-h)\tan\theta(1-\cos\phi)\sin\theta,\\
&y\ell_1=-y\ell_2=H\tan\theta\sin\phi,\quad y\ell_3=-y\ell_4=(H-h)\tan\theta\sin\phi,\\
&z\ell_1=z\ell_2=H\sin\theta(1-\cos\phi),\quad z\ell_3=z\ell_4=(H-h)\sin\theta(1-\cos\phi),
\end{aligned} \tag{3}$$

while the corresponding lengths ℓ_{0i} at the initial unstressed imperfect configuration are readily found, upon substitution of u, υ, w with u_0, υ_0, w_0 in the formulas given above.

Hence, the translational displacements δ_i of the springs are equal to

$$\delta_i = \ell_{\mathrm{D}i} - \ell_{0i}, \quad i = 1\text{–}3 \text{ (SCM)} - i = 1\text{–}4 \text{ (CSPM)}. \tag{4}$$

4. Mathematical analysis

Using $q_1 = u$, $q_2 = \upsilon$ and $q_3 = w$ as generalized coordinates and assuming that both systems are initially ($t = 0$) at rest, the Lagrange equations governing the motion under the action of the step point loading $P(t)$ of infinite duration are given by the well-known relation

$$\frac{\mathrm{d}}{\mathrm{d}t}\left\{\frac{\partial K}{\partial \dot{q}_i}\right\} - \frac{\partial K}{\partial q_i} + \frac{\partial V}{\partial q_i} + \frac{\partial F}{\partial \dot{q}_i} = 0 \quad (i = 1, 2, 3), \tag{5}$$

K is the positive definite function of the kinetic energy and F, the also positive definite dissipation function of Rayleigh, with the following analytical expressions:

$$K = \tfrac{1}{2}m(\dot{u}^2 + \dot{\upsilon}^2 + \dot{w}^2), \tag{6}$$

$$F = \frac{1}{2}\sum_{i=1}^{j} c_i \dot{\delta}_i^2, \quad j = 3 \text{ for SPM}, \quad j = 4 \text{ for CPSM}, \tag{7}$$

while $V = U + \Omega$ is the total potential energy, where U is the elastic strain energy and Ω the potential energy of the external (conservative) load P. Clearly,

$$U = \frac{1}{2}\sum_{i=1}^{j} k_i \delta_i^2, \quad j = 3 \text{ or } 4, \tag{8}$$

$$\Omega = -P(w - w_0). \tag{9}$$

For the preceding loading type, Eq. (5) is associated with the following set of initial conditions:

$$\begin{aligned} &q_i(0) = q_{i0} \quad (q_{10} = u_0,\ q_{20} = \upsilon_0,\ q_{30} = w_0), \\ &\dot{q}_i(0) = 0 \quad (i = 1, 2, 3). \end{aligned} \tag{10}$$

With the aid of relations (4) and (6)–(9), setting $x_1 = q_1$, $x_2 = q_2$, $x_3 = q_3$, $x_4 = \dot{q}_1$, $x_5 = \dot{q}_2$, $x_6 = \dot{q}_3$, the system of Eq. (5) and the initial conditions can be written in a matrix–vector form as follows:

$$\begin{aligned} &\dot{\mathbf{x}} = f(\mathbf{x}; \mathrm{K}, \mathrm{C}, \mathrm{M}; \lambda), \quad \mathbf{x} \in \mathrm{E}^6,\ \ \mathrm{K}, \mathrm{C}, \mathrm{M} \in \mathrm{E}^3,\ \ \lambda \in \mathrm{E}, \\ &\mathbf{x}(x = 0) = \mathbf{x_0}, \quad \dot{\mathbf{x}}(t = 0) = 0 \end{aligned} \tag{11}$$

with the loading λ being the main control parameter.

This defines a highly nonlinear initial-value problem and can be treated as the state equation of a sixth order autonomous nonlinear dynamical system with vector field $\mathbf{x} : R^6 \to R^6$, K being the stiffness parameter vector, M, the concentrated mass vector, and C, the dissipation coefficients vector. It is in fact a damped Hamiltonian system, and thus the only steady-state behavior is the equilibrium (fixed) point $\mathbf{x}_{\mathrm{E}}$, not affected by damping and given by

$$f(\mathbf{x}_{\mathrm{E}}) = 0 \tag{12}$$

from which Eq. (11) yields

$$\frac{\partial V}{\partial x_i}(x_i;\lambda)=0, \quad (i=1,2,3) \tag{13}$$

constituting a necessary and sufficient criterion for static equilibrium.

After introduction of the nondimensional parameters,

$$\begin{aligned} &\bar{q}_i=\frac{q_i}{\ell}, \quad \bar{q}_{i0}=\frac{q_{i0}}{\ell} \ \ (i=1,2,3), \quad \bar{h}=\frac{h}{\ell}, \quad \bar{r}=\frac{r}{\ell}(\bar{h}^2+\bar{r}^2=1),\\ &\overset{*}{c}=c/\sqrt{km}, \quad \tau=\sqrt{\frac{k}{m}}t, \quad \lambda=\frac{P}{k\ell} \ \text{ for SCM}, \end{aligned} \tag{14}$$

and

$$\begin{aligned} &\bar{q}=\frac{q_i}{h}, \quad \bar{q}_{i0}=\frac{q_{i0}}{h}, \quad \bar{k}_i=\frac{k_i}{k_1} \ \ (i=1,2,3),\\ &\bar{x}\ell_i=\frac{x\ell_i}{h}, \quad \bar{y}\ell_i=\frac{y\ell_i}{h}, \quad \bar{z}\ell_i=\frac{z\ell_i}{h} \ \ (i=1,2,3),\\ &\bar{c}_i=c_i/\sqrt{k_1 m}, \quad \tau=\sqrt{\frac{k_1}{m}}t, \quad \lambda=\frac{P}{k_1 h} \ \text{ for CPSM}, \end{aligned} \tag{15}$$

the vector field in Eq. (11) transforms into its proper dimensionless form which is given for each model in Appendix A. This can be solved only numerically, as pointed out in a later discussion. A very efficient procedure is the easily programmable Runge–Kutta–Verner seventh order modified scheme, since with the appropriate choice of a small step h, the error is $O(h^7)$ and thus the method produces reliable information even for large time solutions.

According to previous widely accepted analyses by Kounadis (1993, 1994), dynamic buckling occurs via a saddle or its neighborhood, satisfying condition $V_T \leqslant 0$. This particular fixed point may belong either to physical postbuckling or to complementary unstable, in fact non-stable, equilibrium paths; if the conditions for the initiation of dynamic buckling are fulfilled, as described in detail in the literature given above, the system's motion escapes through the vicinity of the saddle and either an unbounded or a bounded point attractor response is finally exhibited. The exact value of the dynamic buckling load λ_{DD}, when damping is accounted for, can be evaluated only numerically, while for typical limit point systems, like the ones dealt with herein, a very good lower bound $\tilde{\lambda}_D$ can be obtained using the zero total potential energy criterion, i.e. by simultaneously solving Eq. (13) with $V_T=0$; if λ_D denotes the exact load for the corresponding non-dissipative system, then the following inequality is valid:

$$\tilde{\lambda}_D<\lambda_D<\lambda_{DD}<\lambda_S<\lambda_C, \tag{16}$$

where λ_S is the limit point load and λ_C the bifurcational load of the perfect system. Furthermore, the need for a more accurate approximation of λ_{DD} arises only if $\tilde{\lambda}_D$ is significantly smaller than λ_S, a phenomenon scarce for systems with more than two degrees of freedom. Additionally, if the geometry of the considered model is suitable, as for shells of revolution, one can determine λ_{DD} following a straightforward fully nonlinear dynamic analysis, as it will be illustrated below. On any event, the very good energy considerations and new dynamic buckling estimates given in the recent work by Kounadis and Sophianopoulos (1996) must be quoted, which deals with a cylindrical shell panel.

5. Numerical results and discussion

In order to offer a more comprehensive field of understanding and explaining the dynamic buckling phenomenon, it is essential to present at first the results of the nonlinear static stability analysis.

5.1. Nonlinear static buckling – spherical cap model

For this model, two characteristic cases are adopted, a "short" one with $\bar{h} = 0.30$ and a "taller" one ($\bar{h} = 0.60$), both being initially imperfect ($\bar{q}_{i0} = 0.01,\ i = 1$–$3$). Solving the nonlinear equilibrium Eq. (13) with respect to $\bar{q}_1, \bar{q}_2$ and λ, by step increasing the value of the displacement in the direction of the external load $\bar{q}_3$, equilibrium paths are established, as plots of the loading λ vs $\bar{q}_i$. These are clearly depicted in Figs. 3 and 4, from which it is perceivable and more or less expected that for both cases considered the model exhibits a limit point instability, occurring for $\bar{h} = 0.30$ at a load λ_S about ten times less than the corresponding one for $\bar{h} = 0.60$. Furthermore, paths $(\bar{q}_1, \lambda)$ and $(\bar{q}_2, \lambda)$ are symmetrical with respect to the

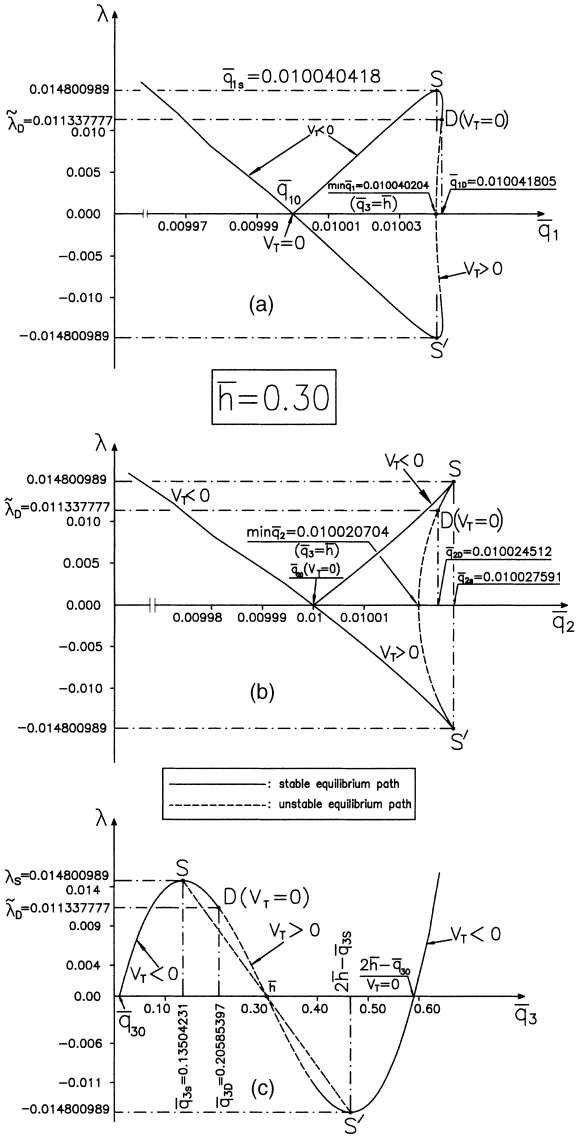

Fig. 3. Physical equilibrium paths $(\bar{q}_i, \lambda; i = 1$–$3)$ of a SCM with $\bar{h} = 0.30$.

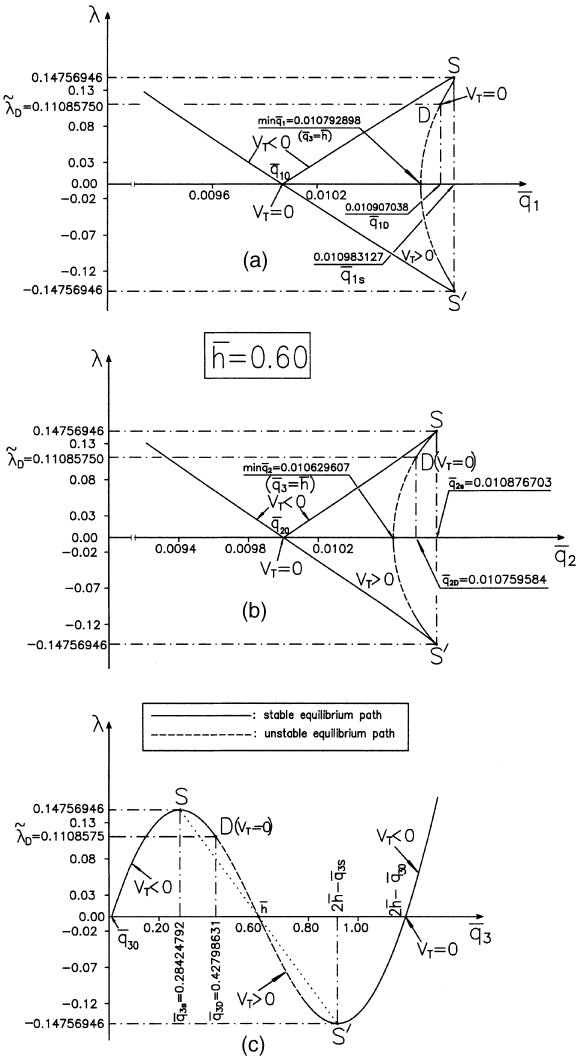

Fig. 4. Physical equilibrium paths $(\bar{q}_i, \lambda; i = 1\text{–}3)$ of a SCM with $\bar{h} = 0.60$.

horizontal axis, while paths $(\bar{q}_3, \lambda)$ of the governing degree of freedom, are fully symmetrical over point $(\bar{h}, 0)$ – ideal snap-through type; at this unstable fixed point all springs lie unstressed without loading on the base of the cap, and both $\bar{q}_1$ and $\bar{q}_2$ experience a local minimum. Their maximum, however, is observed just after limit point S and just before its "mirror" point S'. Thus the "umbrella" reverse geometry snap through is identified, which is one of the main features of actual spherical caps. It should be also noted, that there also exist complementary equilibrium configurations, not presented in Figs. 3 and 4, since their role on the global dynamic response is minimal, as it will be shown in the nonlinear dynamic buckling section.

5.2. Nonlinear static buckling – conical shell panel model

Aiming to cover the most common cases of conical shell panels and to gain the ability of comparison with existing previous analyses, three initially imperfect models are been manipulated, with springs of equal

stiffness and damping ($\bar{q}_{i0} = 0.01,\ i = 1,2,3,\ \bar{k}_i = 1,\ \bar{c}_i = 0.05,\ i = 1$–$4$), implying isotropic elastic characteristics, without any serious loss of generality. Their corresponding projections on the vertical plane through the cone's generator is shown in Fig. 5, from which one can see that case 1 ($\theta = 0.10°,\ \phi = 90°,\ H = 5000$ m, $h = 50$ m) corresponds to a CSPM, very close geometrically to a cylindrical one. Case 2 ($\theta = 1°,\ \phi = 60°,\ H = 58$ m, $h = 1.00$ m) represents a relatively deep conical shell panel, while case 3 ($\theta = 40°,\ \phi = 60°,\ H = 80$ m, $h = 20$ m) is of an average geometry, found excessively in everyday practice.

Following the same procedure as the one outlined for the SCM, natural equilibrium paths ($\bar{q}_i, \lambda,\ i = 1$–$3$) are found and represented schematically within Figs. 6–8. Similarly to SCM, complementary (physically not accepted) equilibria do exist, but again they do not affect the long term response, as it will be specified below.

Comparing the nonlinear static response of the cases mentioned above, the following are observed:

- Evidently, a limit point instability is exhibited throughout, a common characteristic of conical shells.
- For cases 2 and 3, simulating pure conical shells of smooth geometry, all respective equilibrium paths are similar to each other, with the longer shell panel model (case 3) having a smaller load-bearing capacity (to about 50%).
- On the other hand, due to its distinct length, deformation $\bar{q}_1$ behaves in a different manner for the cylinder-like CSPM of case 1, and consequently the governing DOF is apparently the vertical one $\bar{q}_3$, as detected in the literature mentioned earlier. Furthermore, the results for a CSPM with $\varphi = 90°$ and $\theta \to 0$ (almost perfect cylinder) are in excellent agreement with the ones presented in the literature for cylindrical shell panels (Kounadis and Sophianopoulos, 1996).

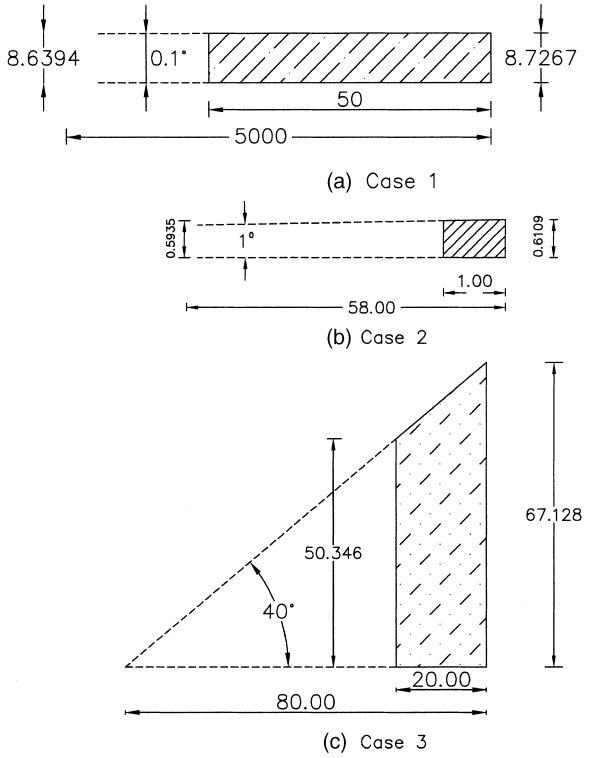

Fig. 5. Three characteristic CSP cases (projections on a vertical plane through the cone's generator).

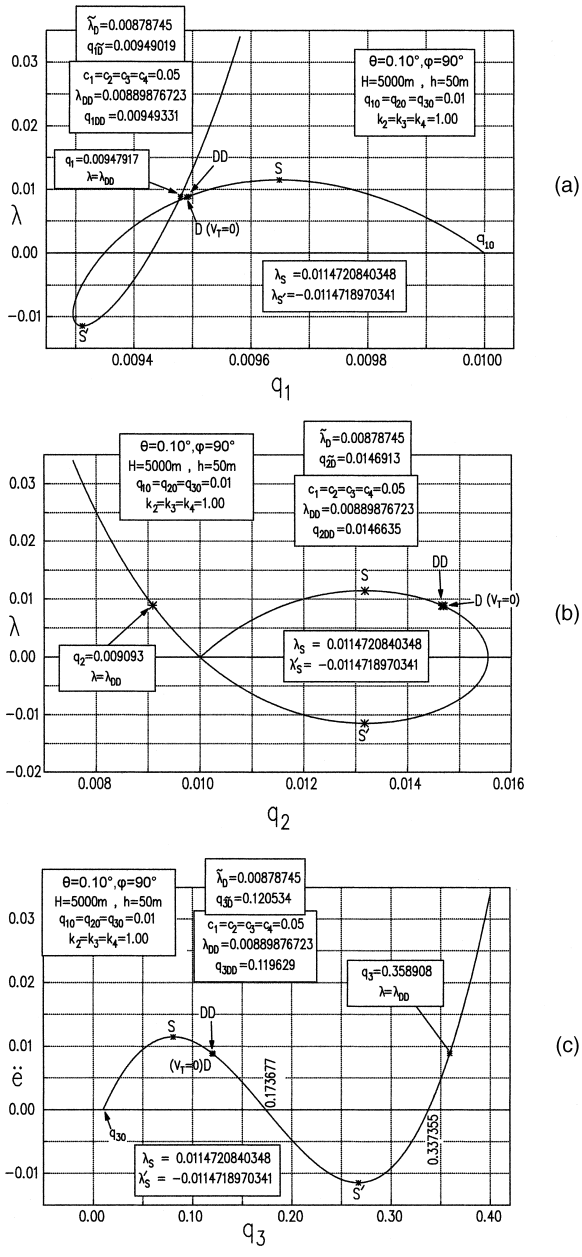

Fig. 6. Physical equilibrium paths $(\bar{q}_i, \lambda;\ i = 1\text{–}3)$ of CSPM case 1.

5.3. Nonlinear dynamic buckling

5.3.1. General observations

Since an exact solution for the strongly nonlinear ordinary differential equations governing the motion of both systems considered is not known, one may either resort to approximate solution techniques or

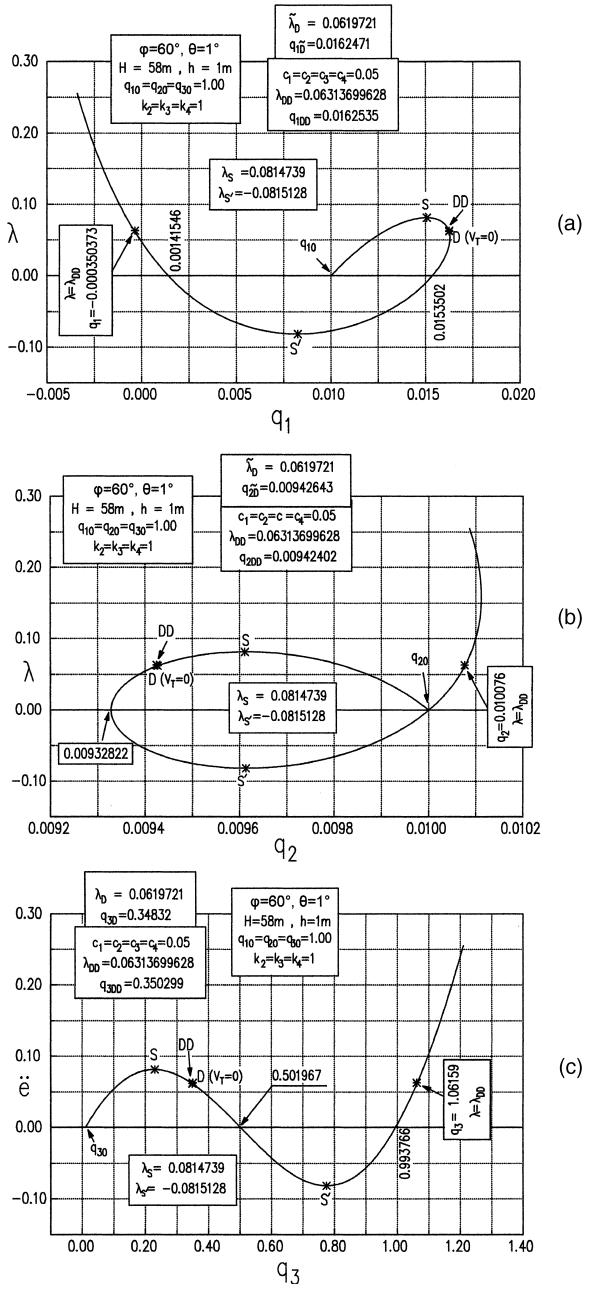

Fig. 7. Physical equilibrium paths $(\bar{q}_i, \lambda;\ i = 1\text{–}3)$ of CSPM case 2.

perform a direct numerical integration. In doing the former, neither standard perturbation methods and variations (Nayfeh, 1973; Nayfeh and Mook, 1979) nor harmonic balancing (Adadan and Huseyin, 1984) are applicable, because the first requires the existence of a basic exact nonlinear solution, while the second produces valuable information when the state variables are of a polynomial form, which are by no means the case for the models under study.

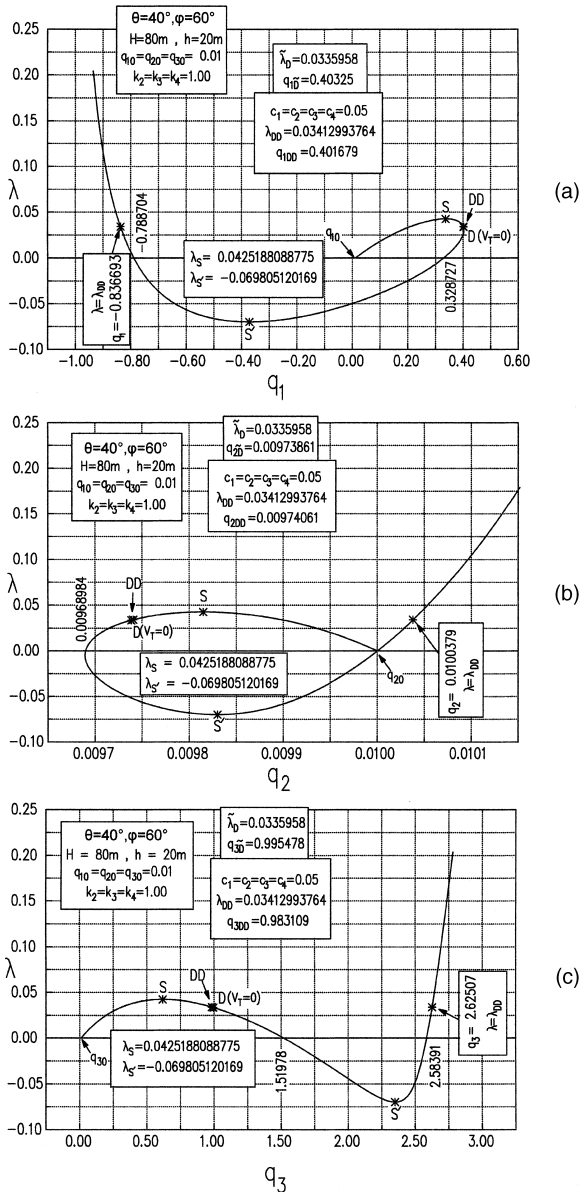

Fig. 8. Physical equilibrium paths $(\bar{q}_i, \lambda;\ i = 1\text{–}3)$ of CSPM case 3.

Moreover, the most governing nonlinear terms in the equations of motion of SCM and CSPM are not a priori known, and trying to reduce the systems' dimensionality via normal forms, leading to unavoidable series expansions and truncating, would rather complicate than simplify the whole analysis. The presence of damping results to energy-balance inequalities and thus the benefit of a first integral of motion without the need of cumbersome linearization, serving as a Lyapunov function is lost (Wiggins, 1990).

Hence, a straightforward fully nonlinear dynamic analysis, by carefully choosing an appropriate numerical scheme, remains the only efficient and reliable tool for the study of motion itself, as well as of the global stability of steady-states, and will be hereafter employed.

5.3.2. Spherical cap model

The shape of the physical primary and secondary equilibrium paths for both cases ($\bar{h} = 0.30, 060$) in Figs. 3 and 4 offer a beforehand indication of the type of dynamic buckling expected. Indeed, it is of a snap-through type, since as depicted in the corresponding phase plane portraits of Figs. 9 and 10, dynamic buckling takes place in the vicinity of a saddle point DD on the unstable postbuckling path with negative total potential, and after bounded oscillations of small amplitude and duration about this fixed point, the motion escapes remaining always bounded, to be finally captured by remote stable natural equilibria, acting as point attractors and implying global dynamic stability. The value of the dynamic buckling load λ_{DD} can be determined numerically with any desired accuracy, based on the mere observation that an escaped motion is initiated if and only if its amplitude for the degree of freedom of the external loading $\bar{q}_3(\tau)$ overrides the barrier of the symmetry plane, i.e. if and only if $\bar{q}_3(\tau) \geqslant \bar{h}$. In this manner, the values of λ_{DD} (for $\overset{*}{c} = 0.06$) are found equal to 0.01147963 ($\bar{h} = 0.30$) and 0.11397747 ($\bar{h} = 0.60$), while the zero total potential criterion yields the lower bound dynamic estimate $\tilde{\lambda}_{\mathrm{D}}$ (note that the saddle point D for $V_T = 0$ is shown in Figs. 3 and 4). The latter values are equal to 0.011337777 and 0.1108575, respectively, revealing a discrepancy – compared to λ_{DD} – of 1.24% and 2.56%, practically negligible, a finding quite useful for engineering design purposes. Hence, no necessity for further approximations of λ_{DD} based on geometric aspects of the motion channel geometry arises, while the significant amplitude of the remaining two less-dominant DOF $\bar{q}_1(\tau)$ and $\bar{q}_2(\tau)$, before the motion after considerable time finally settles on its attractor, can be conveniently interpreted as the effect of complementary equilibria, which do not act as attractors, as reported for other multi-DOF systems.

5.3.3. Conical shell panel model

Following a similar procedure as with SCM it is found that the dynamic buckling mechanism is again of a snap-through type, associated with a point attractor response in the large, as illustrated in the phase plane portraits of Figs. 11–13 for cases 1–3, respectively. For the dominant degree of freedom the motion after escaping close to the saddle DD is instantly captured by its attractor; on the other hand the oscillations after dynamic buckling of $\bar{q}_1(\tau)$ and $\bar{q}_2(\tau)$ are quite complicated, implying a more significant intermediate effect of complementary equilibria, equivalent to a non-smooth energy hypersurface with multiple relative maxima and minima.

Additionally, the zero total potential criterion yields lower bound dynamic estimates of very good accuracy, since the maximum difference calculated between $\tilde{\lambda}_{\mathrm{D}}$ and λ_{DD} is 1.84%; hence, the relevant conclusions drawn in the SCM dynamic buckling analysis are valid also for the CSPM.

For both models considered, the qualitative findings concerning dynamic instability via snap through are found closely matching the ones obtained recently (Ye and Zhiming, 1997) for parametrically excited thin spherical and conical shells.

6. Conclusions

The most important conclusions of the present study are as follows:

(a) The dynamic buckling response of elastic shell panels of revolution with significant membrane action and especially spherical and conical ones, under step loading, can be comprehensively presented through efficient simple one-mass 3-DOF imperfect dissipative models.

(b) The dynamic snap-through buckling mechanism, being the main feature of actual shell panels, is captured by the proposed simulations, while the zero total potential criterion yields excellent approximations of the exact dynamic buckling load, of major importance for structural design purposes.

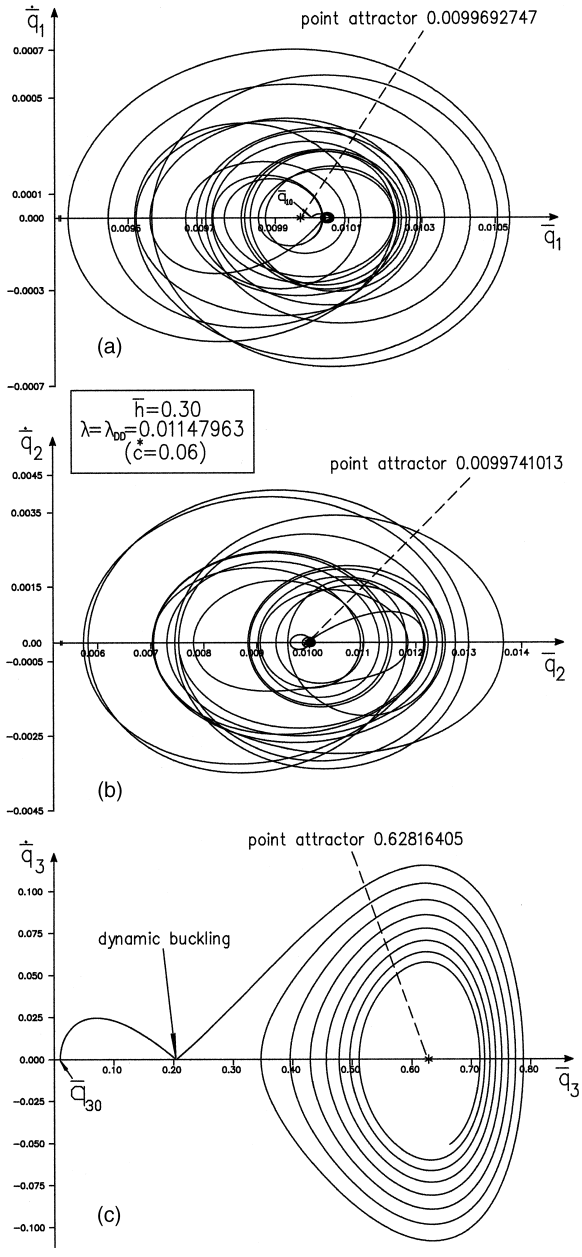

Fig. 9. Phase plane portraits $[\bar{q}_i(\tau), \dot{\bar{q}}_i(\tau);\ i = 1\text{–}3]$ of a SCM with $\bar{h} = 0.30$, $\overset{*}{c} = 0.06$ at $\lambda = \lambda_{\mathrm{DD}} = 0.01147963$.

(c) The presence of complementary equilibrium configurations only complicates the oscillations and delays the inevitable effect of the remote stable point attractor, thus being not significant for the systems global response.
(d) Finally, contrary to previous findings, the motion of the systems after dynamic buckling is not of a chaotic nature.

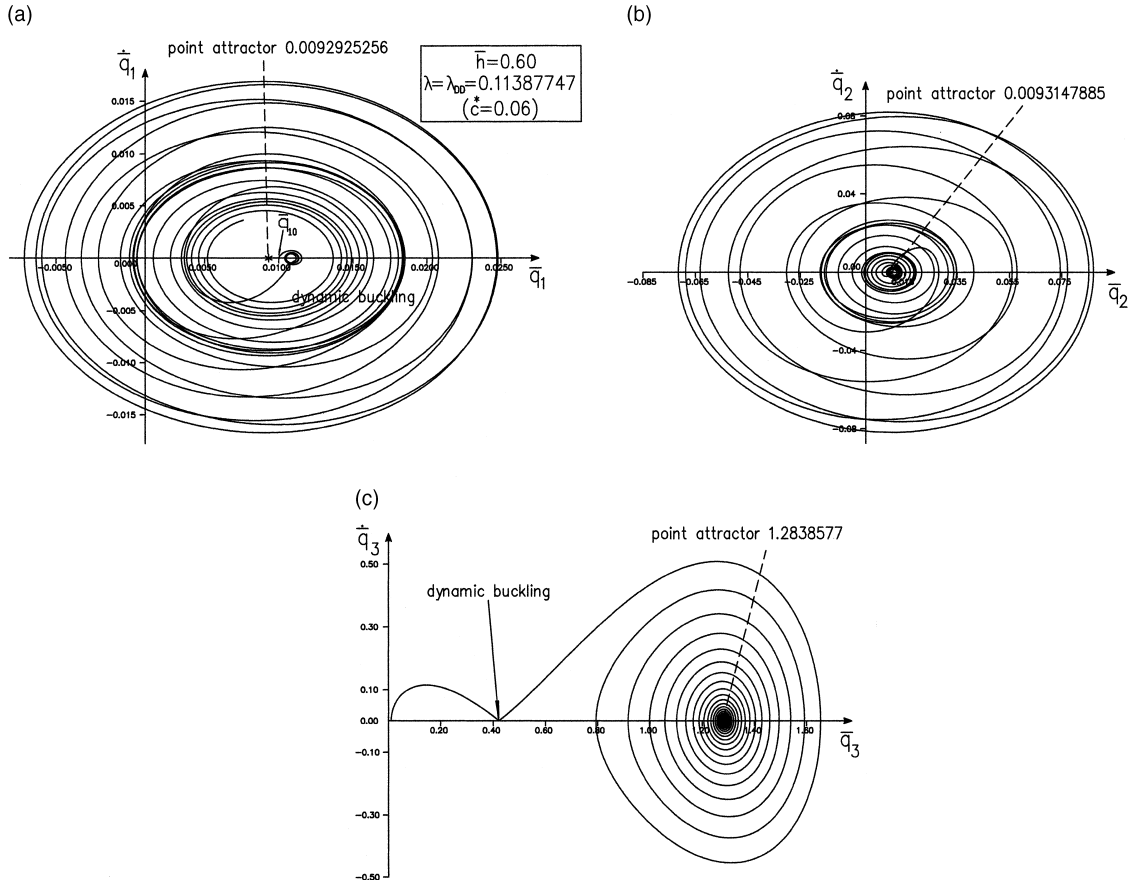

Fig. 10. Phase plane portraits $[\bar{q}_i(\tau), \dot{\bar{q}}_i(\tau);\ i = 1\text{–}3]$ of a SCM with $\bar{h} = 0.60$, $\overset{*}{c} = 0.06$ at $\lambda = \lambda_{DD} = 0.11387747$.

Appendix A. Differential equations of motion, static equilibrium equations and total potential energy in dimensionless form

A.1. Spherical cap model

$$\dot{x}_4 = -\frac{\partial \bar{V}_T}{\partial x_1} - x_4^* c \left\{ \frac{x_1^2}{\bar{\ell}_{D1}^2} + \frac{\left(\bar{r}\frac{\sqrt{3}}{2} - x_1\right)^2}{\bar{\ell}_{D2}^2} + \frac{\left(\bar{r}\frac{\sqrt{3}}{2} + x_1\right)^2}{\bar{\ell}_{D3}^2} \right\}$$
$$- x_5^* c \left\{ -\frac{\left(\bar{r} - x_2\right)}{\bar{\ell}_{D1}^2} - \frac{\left(\frac{\bar{r}}{2} + x_2\right)\left(\bar{r}\frac{\sqrt{3}}{2} - x_1\right)}{\bar{\ell}_{D2}^2} + \frac{\left(\frac{\bar{r}}{2} + x_2\right)\left(\bar{r}\frac{\sqrt{3}}{2} + x_1\right)}{\bar{\ell}_{D3}^2} \right\}$$
$$- x_6^* c \left\{ -\frac{x_1}{\bar{\ell}_{D1}} + \frac{\left(\bar{r}\frac{\sqrt{3}}{2} - x_1\right)}{\bar{\ell}_{D2}} + \frac{\left(\bar{r}\frac{\sqrt{3}}{2} + x_1\right)}{\bar{\ell}_{D3}} \right\} (\bar{h} - x_3) = 0, \tag{A.1}$$

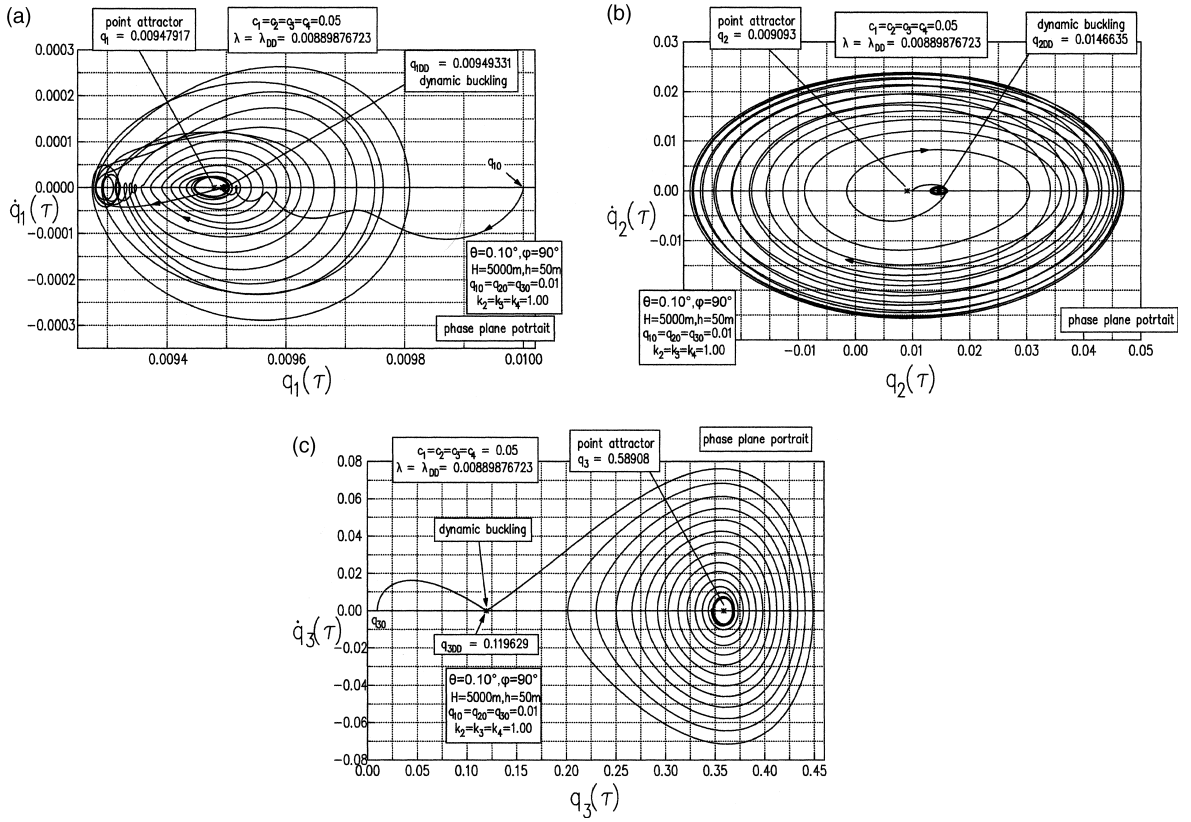

Fig. 11. Phase plane portraits $[\bar{q}_i(\tau), \dot{\bar{q}}_i(\tau);\ i = 1\text{–}3]$ of CSPM case 1 with $\bar{c}_i = 0.05,\ i = 1\text{–}4$ at $\lambda = \lambda_{\mathrm{DD}} = 0.00889876723$.

$$\dot{x}_5 = -\frac{\partial \bar{V}_T}{\partial x_2} + x_4^* c^* \left\{ -\frac{x_1\left(\bar{r} - x_2\right)}{\bar{\ell}_{\mathrm{D2}}^2} - \frac{\left(\bar{r}\frac{\sqrt{3}}{2} - x_1\right)\left(\frac{\bar{r}}{2} + x_2\right)}{\bar{\ell}_{\mathrm{D2}}^2} + \frac{\left(\bar{r}\frac{\sqrt{3}}{2} + x_1\right)\left(\frac{\bar{r}}{2} + x_2\right)}{\bar{\ell}_{\mathrm{D3}}^2} \right\}$$
$$- x_5^* c^* \left\{ -\frac{\left(\bar{r} - x_2\right)^2}{\bar{\ell}_{\mathrm{D1}}^2} + \frac{\left(\frac{\bar{r}}{2} + x_2\right)^2}{\bar{\ell}_{\mathrm{D2}}^2} + \frac{\left(\frac{\bar{r}}{2} + x_2\right)^2}{\bar{\ell}_{\mathrm{D3}}^2} \right\}$$
$$- x_6^* c^* \left\{ -\frac{\left(\bar{r} - x_2\right)}{\bar{\ell}_{\mathrm{D1}}^2} - \frac{\left(\frac{\bar{r}}{2} + x_2\right)}{\bar{\ell}_{\mathrm{D2}}^2} + \frac{\left(\frac{\bar{r}}{2} + x_2\right)}{\bar{\ell}_{\mathrm{D3}}^2} \right\} (\bar{h} - x_3) = 0, \tag{A.2}$$

$$\dot{x}_6 = -\frac{\partial \bar{V}_T}{\partial x_3} + x_4^* c^* \left\{ \frac{x_1}{\bar{\ell}_{\mathrm{D2}}^2} - \frac{\left(\bar{r}\frac{\sqrt{3}}{2} - x_1\right)}{\bar{\ell}_{\mathrm{D2}}^2} + \frac{\left(\bar{r}\frac{\sqrt{3}}{2} + x_1\right)}{\bar{\ell}_{\mathrm{D3}}^2} \right\} (\bar{h} - x_3)$$
$$+ x_5^* c^* \left\{ -\frac{\left(\bar{r} - x_2\right)}{\bar{\ell}_{\mathrm{D1}}^2} + \frac{\left(\frac{\bar{r}}{2} + x_2\right)}{\bar{\ell}_{\mathrm{D2}}^2} + \frac{\left(\frac{\bar{r}}{2} + x_2\right)}{\bar{\ell}_{\mathrm{D3}}^2} \right\} (\bar{h} - x_3)$$
$$- x_6^* c^* \left\{ \frac{1}{\bar{\ell}_{\mathrm{D1}}^2} + \frac{1}{\bar{\ell}_{\mathrm{D2}}^2} + \frac{1}{\bar{\ell}_{\mathrm{D3}}^2} \right\} \left(\bar{h} - x_3\right)^2 = 0, \tag{A.3}$$

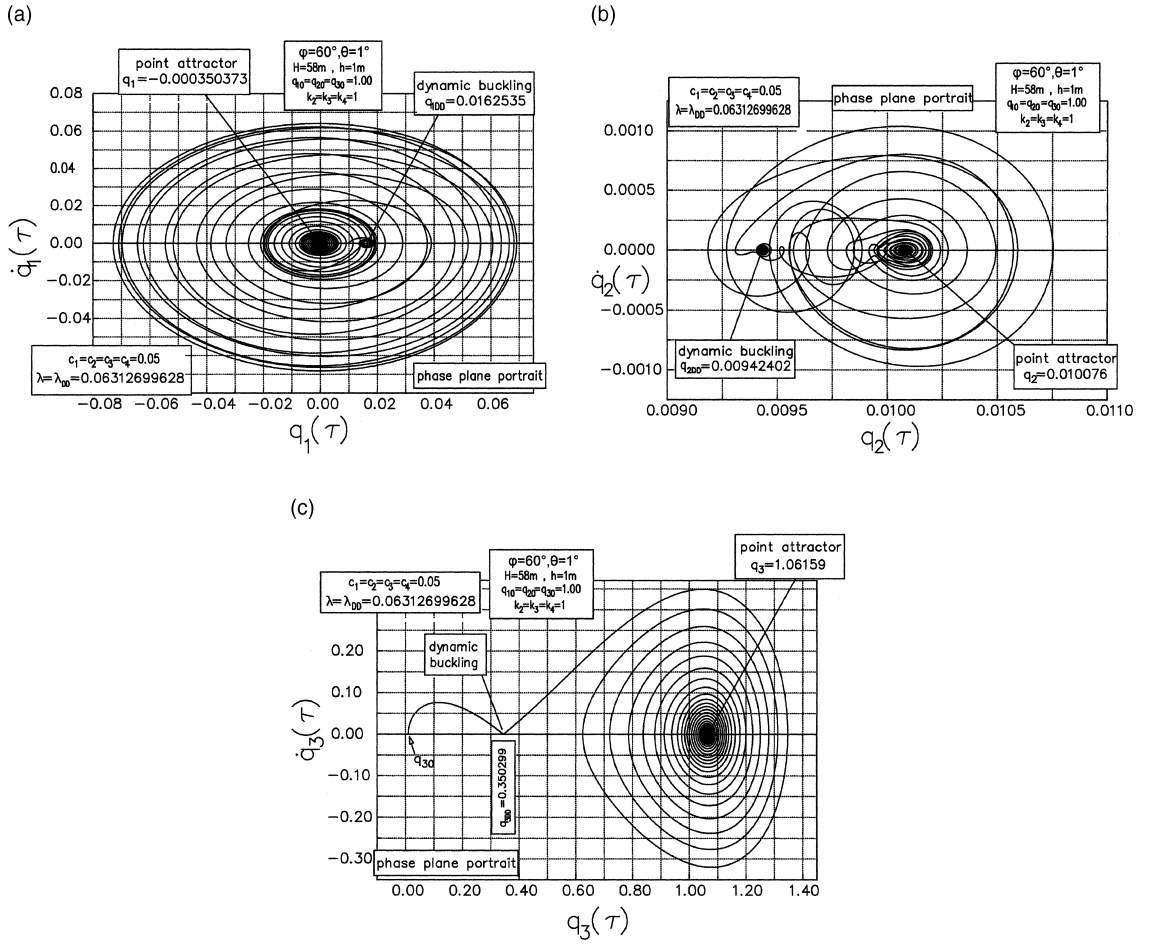

Fig. 12. Phase plane portraits $[\bar{q}_i(\tau), \dot{\bar{q}}_i(\tau);\ i = 1\text{–}3]$ of CSPM case 2 with $\bar{c}_i = 0.05,\ i = 1\text{–}4$ at $\lambda = \lambda_{\mathrm{DD}} = 0.06312699628$.

where

$$\frac{\partial \bar{V}_T}{\partial x_1} = \left\{1 - \frac{\beta_1}{\bar{\ell}_{\mathrm{D1}}}\right\} x_1 - \left\{1 - \frac{\beta_2}{\bar{\ell}_{\mathrm{D2}}}\right\}\left(\frac{\bar{r}\sqrt{3}}{2} - x_1\right) + \left\{1 - \frac{\beta_3}{\bar{\ell}_{\mathrm{D3}}}\right\}\left(\frac{\bar{r}\sqrt{3}}{2} + x_1\right), \tag{A.4}$$

$$\frac{\partial \bar{V}_T}{\partial x_2} = -\left\{1 - \frac{\beta_1}{\bar{\ell}_{\mathrm{D1}}}\right\}(\bar{r} - x_2) + \left\{1 - \frac{\beta_2}{\bar{\ell}_{\mathrm{D2}}}\right\}\left(\frac{\bar{r}}{2} + x_2\right) + \left\{1 - \frac{\beta_3}{\bar{\ell}_{\mathrm{D3}}}\right\}\left(\frac{\bar{r}}{2} + x_2\right), \tag{A.5}$$

$$\frac{\partial \bar{V}_T}{\partial x_3} = -\left\{3 - \frac{\beta_1}{\bar{\ell}_{\mathrm{D1}}} - \frac{\beta_2}{\bar{\ell}_{\mathrm{D2}}} - \frac{\beta_3}{\bar{\ell}_{\mathrm{D3}}}\right\}(\bar{h} - x_3) - \lambda \tag{A.6}$$

with

$$\bar{\ell}_{\mathrm{D}i} = \ell_{\mathrm{D}i}/\ell \text{ from expressions (1) and } \beta_i = \ell_{0i}/\ell\ (i = 1, 2, 3),$$
$$\bar{V}_T = \frac{V_T}{k\ell^2} = \frac{1}{2}\sum_{i=1}^{3}\left(\bar{\ell}_{\mathrm{D}i} - \beta_i\right)^2 - \lambda(x_3 - x_{30}). \tag{A.7}$$

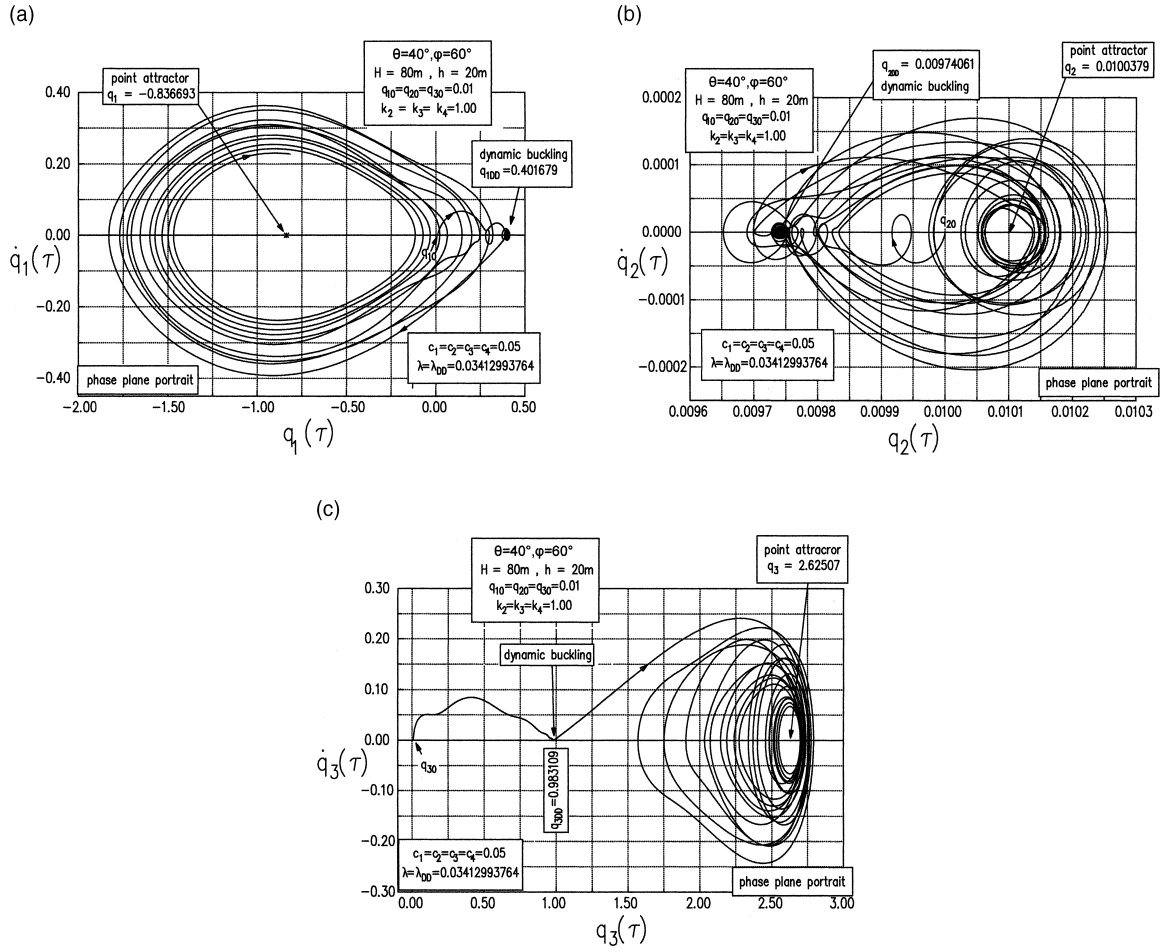

Fig. 13. Phase plane portraits $[\bar{q}_i(\tau), \dot{\bar{q}}_i(\tau);\ i = 1\text{–}3]$ of CSPM case 3 with $\bar{c}_i = 0.05,\ i = 1\text{–}4$ at $\lambda = \lambda_{\mathrm{DD}} = 0.03412993764$.

A.2. Conical shell panel model

$$\dot{x}_4 = -\frac{\partial \bar{V}_T}{\partial x_1} + \sum_{i=1}^{4} R_i \frac{\bar{x}\ell_i - x_1}{\bar{\ell}_{\mathrm{D}i}}, \tag{A.8}$$

$$\dot{x}_5 = -\frac{\partial \bar{V}_T}{\partial x_2} + \sum_{i=1}^{4} R_i \frac{\bar{y}\ell_i - x_2}{\bar{\ell}_{\mathrm{D}i}}, \tag{A.9}$$

$$\dot{x}_6 = -\frac{\partial \bar{V}_T}{\partial x_3} + \sum_{i=1}^{4} R_i \frac{\bar{z}\ell_i - x_3}{\bar{\ell}_{\mathrm{D}i}}, \tag{A.10}$$

where

$$R_i = -\bar{c}_i \frac{\left(\bar{x}\ell_i - x_1\right)x_4 + \left(\bar{y}\ell_i - x_2\right)x_5 + \left(\bar{z}\ell_i - x_3\right)x_6}{\bar{\ell}_{\mathrm{D}i}} \quad (i = 1,2,3), \tag{A.11}$$

$$\frac{\partial \bar{V}_T}{\partial x_1} = -\sum_{i=1}^{4} \bar{k}_i \left\{1 - \frac{\beta_i}{\bar{\ell}_{\mathrm{D}i}}\right\}(\bar{x}\ell_i - x_1), \tag{A.12}$$

$$\frac{\partial \bar{V}_T}{\partial x_2} = -\sum_{i=1}^{4} \bar{k}_i \left\{1 - \frac{\beta_i}{\bar{\ell}_{\mathrm{D}i}}\right\}(\bar{y}\ell_i - x_2), \tag{A.13}$$

$$\frac{\partial \bar{V}_T}{\partial x_3} = -\sum_{i=1}^{4} \bar{k}_i \left\{1 - \frac{\beta_i}{\bar{\ell}_{\mathrm{D}i}}\right\}(\bar{z}\ell_i - x_3) \tag{A.14}$$

with

$$\begin{aligned} &\bar{\ell}_{\mathrm{D}i} = \ell_{\mathrm{D}i}/h \text{ from expressions (2) and } \beta_i = \ell_{0i}/h \ (i = 1,2,3), \\ &\bar{V}_T = \frac{V_T}{k_1 h^2} = \frac{1}{2}\sum_{i=1}^{4}\left(\bar{\ell}_{\mathrm{D}i} - \beta_i\right)^2 - \lambda(x_3 - x_{30}). \end{aligned} \tag{A.15}$$

In all the relations given above

$$x_i = \bar{q}_i, \quad x_{i0} = \bar{q}_{i0} \text{ and } \quad x_{\mathrm{j}} = \dot{\bar{q}}_i, \quad i = 1,2,3 \leftrightarrow \ j = 4,5,6. \tag{A.16}$$

References

Adadan, A., Huseyin, K., 1984. An intrinsic method of harmonic analysis for non-linear oscillations: a perturbation technique. Journal of Sound and Vibration 95 (4), 525–530.

Akkas, N., 1976. Bifurcation and snap-through phenomena in asymmetric dynamic analysis of shallow spherical shells. Computers and Structures 6, 241–251.

Akkas, N., 1978. On the dynamic snap-out instability of inflated nonlinear spherical membranes. International Journal of Non-Linear Mechanics 13, 177–183.

Chien, L.S., Palazotto, A.N., 1992. Dynamic buckling of composite cylindrical panels with high-order transverse shears subjected to a transverse concentrated load. International Journal of Non-Linear Mechanics 27 (5), 719–734.

Galladine, C.R., 1995. Understanding imperfection-sensitivity in the buckling of thin-walled shells. Thin Walled Structures 23, 215–235.

Greer, J.M., Palazotto, A.N., 1995. Nonlinear dynamics of simple shell model with chaotic snapping behavior. Journal of Engineering Mechanics 121 (6), 753–761.

Karaesmen, E., Ileri, L., Akkas, N., 1992. Chaotic dynamic analysis of viscoelastic shallow spherical shells. Computers and Structures 44 (4), 851–857.

Kounadis, A.N., 1993. Static and dynamic, local and global, bifurcations in nonlinear autonomous structural systems. AIAA Journal 31 (8), 1468–1477.

Kounadis, A.N., 1996. Qualitative criteria in nonlinear dynamic buckling and stability of autonomous dissipative systems. International Journal of Non-Linear Mechanics 31 (6), 887–906.

Kounadis, A.N., 1994. A qualitative analysis of the local and global dynamic buckling and stability of autonomous discrete systems. Quarterly Journal of Mechanics and Applied Mathematics 47 (2), 269–295.

Kounadis, A.N., Sophianopoulos, D.S., 1996. Nonlinear dynamic buckling of a cylindrical shell panel model. AIAA Journal 34 (11), 2421–2428.

Libai, A., Simmonds, J.G., 1998. The Nonlinear Theory of Elastic Shells. Cambridge University Press, Cambridge.

Michaltsos, G.T., Ermopoulos, I.C., Sophianopoulos, D.S., 1996. Modeling of the non-linear response of a spherical shell. In: Proceedings of the Second International Conference on Coupled Instabilities in Metal Structures. Liege, Belgium, pp. 491–498.

Michaltsos, G.T., Sophianopoulos, D.S., Konstandakopoulos, T.G., 1998. Non-linear buckling response of a conical shell panel. In: Proceedings of the Fourth International Conference on Computational Structures Technology. Edinburgh, Scotland, Advances in Finite Element Procedures and Techniques. Civil Comp Press, Edinburgh, UK. pp. 239–246.

Nayfeh, A.H., 1973. Perturbation Methods. Wiley, New York.

Nayfeh, A.H., Mook, D.T., 1979. Non-Linear Oscillations. Wiley-Interscience, New York.

Simitses, G.J., 1990. Dynamic Stability of Suddenly Loaded Structures. Springer, New York.

Wiggins, St., 1990. Introduction to Applied Nonlinear Dynamical Systems and Chaos. Springer, New York.

Ye, Zhiming, 1997. The non-linear vibration and dynamic instability of thin shallow shells. Journal of Sound and Vibration 202 (3), 303–311.

Ye, Zhiming, Han, R.P.S., 1995. On the nonlinear analysis of orthotropic shallow shells of revolution. Computers and Structures 55 (2), 325–331.